

# Nanoscale

Accepted Manuscript

This article can be cited before page numbers have been issued, to do this please use: Z. Liu, M. S. Islam, Y. Fang, M. Zhu, C. C. Cao and G. Xu, *Nanoscale*, 2025, DOI: 10.1039/D4NR04583A.



This is an Accepted Manuscript, which has been through the Royal Society of Chemistry peer review process and has been accepted for publication.

Accepted Manuscripts are published online shortly after acceptance, before technical editing, formatting and proof reading. Using this free service, authors can make their results available to the community, in citable form, before we publish the edited article. We will replace this Accepted Manuscript with the edited and formatted Advance Article as soon as it is available.

You can find more information about Accepted Manuscripts in the [Information for Authors](#).

Please note that technical editing may introduce minor changes to the text and/or graphics, which may alter content. The journal's standard [Terms & Conditions](#) and the [Ethical guidelines](#) still apply. In no event shall the Royal Society of Chemistry be held responsible for any errors or omissions in this Accepted Manuscript or any consequences arising from the use of any information it contains.

# 1 **Design Strategies and Performance Enhancements of PVDF-based Flexible Electrolytes** 2 **for High-Performance All-Solid-State Lithium Metal Batteries**

3 Zhongxiu Liu<sup>1,2,3</sup>, Md Shariful Islam<sup>4</sup>, Yuhui Fang<sup>5</sup>, Meifang Zhu<sup>1</sup>, Changyong (Chase)  
4 Cao<sup>4,6\*</sup>, Guiyin Xu<sup>1\*</sup>

5 <sup>1</sup> *State Key Laboratory for Modification of Chemical Fibers and Polymer Materials, College*  
6 *of Materials Science and Engineering, Donghua University, Shanghai 201620, China*

7 <sup>2</sup> *Henan Academy of Sciences, Zhengzhou 450001, China*

8 <sup>3</sup> *School of Materials Science and Engineering, Zhengzhou University, Zhengzhou 450001,*  
9 *China*

10 <sup>4</sup> *Laboratory for Soft Machines and Electronics, Department of Mechanical and Aerospace*  
11 *Engineering, Case Western Reserve University, Cleveland, OH 44106, USA*

12 <sup>5</sup> *4D Maker LLC, Okemos, MI 44106, USA*

13 <sup>6</sup> *Advanced Platform Technology (APT) Center, Louis Stokes Cleveland VA Medical Center,*  
14 *Cleveland, OH 44106, USA*

## 16 **Abstract**

17 Lithium metal is considered one of the most promising anode materials for lithium batteries  
18 due to its high theoretical specific capacity (3860 mAh·g<sup>-1</sup>) and low redox potential (-3.04 V).  
19 However, uncontrolled lithium dendrite growth and severe interfacial side reactions during  
20 cycling result in poor performance and safety risks, significantly limiting its practical  
21 applications. Replacing liquid electrolytes with solid polymer electrolytes (SPEs) offers a  
22 solution, as SPEs provide flexibility and good electrode compatibility, effectively inhibiting  
23 dendrite growth and reducing interfacial reactions. Among SPEs, poly(vinylidene fluoride)  
24 (PVDF)-based solid electrolytes offer excellent thermal stability and mechanical strength,  
25 making them highly suitable for high-energy-density flexible batteries. This review presents  
26 recent advances in PVDF-based solid-state electrolytes (SSEs) for stable, high-performance  
27 lithium metal batteries (LMBs). We focus on modification strategies that enhance the  
28 performance of PVDF-based SSEs in solid-state LMBs and highlight how synthesis methods,  
29 nano/microstructural design, and electrochemical properties are interrelated. Lastly, we discuss  
30 the challenges and prospects for PVDF-based SSEs in next-generation high-performance  
31 LMBs.

32 **Keywords:** poly(vinylidene-fluoride) (PVDF), Li metal battery, solid state electrolyte (SSE),  
33 Flexible Electrolyte, solid polymer electrolytes (SPEs)



## 34 1. Introduction

35 Renewable energy sources, including solar, wind, and wave energy, have become  
36 increasingly attractive due to the urgency posed by climate change and environmental pollution  
37 associated with traditional energy sources.<sup>1-5</sup> However, effectively harnessing these renewable  
38 energies remains challenging due to their intermittent and discontinuous nature. Consequently,  
39 energy storage devices, particularly rechargeable batteries, are in high demand as they hold  
40 substantial potential to mitigate these issues.<sup>6,7</sup> Among various rechargeable batteries, lithium-  
41 ion batteries (LIBs) have gained widespread attention for their long life and environmental  
42 benefits.<sup>8,9</sup> Nevertheless, commercial LIBs, which use graphite as the anode, have undergone  
43 extensive development over the past three decades, nearing their theoretical performance limits  
44 and struggling to meet the future demand for high-energy-density storage.<sup>10</sup> Therefore, there is  
45 an urgent need to explore new battery systems and materials to achieve higher energy densities.

46 Compared to commercial lithium-ion batteries, lithium metal batteries (LMBs), which use  
47 metallic lithium directly as the anode, offer higher specific energy based on the electroplating  
48 and stripping of lithium ions.<sup>11</sup> Lithium metal has an exceptionally high theoretical specific  
49 capacity (3860 mAh g<sup>-1</sup>) and a very low reduction potential (-3.04 V),<sup>12</sup> making LMBs with  
50 lithium metal anodes highly promising for achieving high energy densities. Additionally,  
51 lithium metal can be used as the anode material directly, eliminating the need for heavy and  
52 inactive current collectors, thus further increasing the battery's specific energy.<sup>13</sup> The lithium  
53 metal anode (LMA) holds significant potential for development and is highly anticipated as a  
54 transformative solution.<sup>14</sup> However, several challenges currently limit its practical  
55 application.<sup>15</sup> Firstly, the volume expansion of the lithium metal anode during cycling causes  
56 instability in the solid electrolyte interface (SEI) layer, leading to reduced coulombic efficiency  
57 and accelerated capacity decay.<sup>16</sup> Secondly, the uncontrolled growth of lithium dendrites can  
58 penetrate the separator, causing short circuits, fire hazards, and other safety risks.<sup>17</sup>

59 Organic liquid electrolytes, characterized by high volatility, flammability, and leakage risks,  
60 pose inherent safety issues for lithium metal batteries.<sup>18</sup> In contrast, replacing liquid  
61 electrolytes with solid-state electrolytes (SSEs) can address these concerns by significantly  
62 improving the safety and energy density of lithium metal batteries.<sup>19,20</sup> Solid electrolytes are



63 typically classified as either inorganic or polymer-based.<sup>21-23</sup> Inorganic SSEs offer excellent  
64 mechanical properties, thermal stability, and high ionic conductivity,<sup>24</sup> with primary examples  
65 including oxides, sulfides, and halides.<sup>25-27</sup> However, large-scale application faces challenges.  
66 Although oxide-based SSEs exhibit relatively high ionic conductivity, their rigidity  
67 complicates battery processing and assembly and increases interface resistance.<sup>28</sup> During  
68 preparation, oxide SSEs often require prolonged high-speed ball milling and elevated  
69 temperatures to enhance uniformity and density, resulting in high manufacturing costs. Sulfide  
70 and halide SSEs, while having ionic conductivities comparable to liquid electrolytes, generally  
71 exhibit narrow electrochemical windows, complicating direct compatibility with high-voltage  
72 cathode materials.<sup>28-31</sup>

73 Polymer-based SSEs, on the other hand, are highly flexible, capable of forming strong  
74 interfacial contact with both cathodes and anodes, and exhibit low interfacial impedance,  
75 offering significant practical potential.<sup>32</sup> Common polymer substrates include poly(ethylene  
76 oxide) (PEO),<sup>33</sup> poly(methyl methacrylate) (PMMA),<sup>34</sup> and poly(vinylidene fluoride)  
77 (PVDF).<sup>35</sup> PVDF, a semi-crystalline polymer with radially crystallized, ball-like structures,  
78 has chain segments that create a dipole moment due to the presence of electro-negative fluorine  
79 and electro-positive hydrogen atoms.<sup>36</sup> This dipole moment grants PVDF a moderate dielectric  
80 constant, facilitating the dissociation of lithium salts in the electrolyte. PVDF has various  
81 crystalline phases, including  $\alpha$  and  $\beta$  phases;  $\alpha$ -phase PVDF provides thermodynamic stability,  
82 while  $\beta$ -phase offers a higher dielectric constant. PVDF-based SSEs are typically prepared by  
83 dissolving PVDF in a solvent, which is then dried and evaporated to form a matrix containing  
84 lithium salt.<sup>35</sup> Research by Nan et al. has shown that the solvent molecules in the PVDF-based  
85 SSE coordinate with lithium ions, facilitating lithium-ion transport by interacting with fluorine  
86 atoms on the PVDF chains.<sup>37, 38</sup> This ability to promote ionic conductivity has made PVDF-  
87 based SSEs attractive for use with lithium metal anodes.

88 This review will summarize recent advances in PVDF-based flexible SSEs for lithium  
89 metal batteries, focusing on modification strategies, electrochemical performance, and design  
90 structures. We will also discuss the preparation and modification methods, the nano- and  
91 microstructures, and the electrochemical properties of PVDF-based SSEs. Finally, we will  
92 provide an outlook on the potential of PVDF-based SSEs for high-performance lithium metal



93 batteries.

View Article Online  
DOI: 10.1039/D4NR04583A

## 94 2. Design Strategies and Properties of PVDF-Based Flexible SSEs in LMBs

95 PVDF exhibits several ideal properties for fabricating solid-state electrolytes,<sup>35</sup> including  
96 1) high mechanical strength and toughness, 2) a wide electrochemical voltage window, 3)  
97 excellent thermal stability - capable of sustained operation at temperatures up to 150°C with a  
98 decomposition threshold around 400°C, and 4) high electrochemical stability with minimal  
99 reactive interference with other materials. These properties contribute to PVDF's ability to  
100 dissociate lithium more efficiently due to its high dielectric constant, which reduces  
101 interactions between ion pairs and facilitates ion transport. With a relative permittivity of 8.3,<sup>35</sup>  
102 PVDF supports a favorable environment for lithium dissociation, aiding in the overall ionic  
103 conductivity of the SSE.

104 By leveraging these intrinsic PVDF properties, researchers have developed various  
105 modification techniques to engineer polymer electrolytes with enhanced and consistent  
106 performance. Key strategies for optimizing PVDF-based SSEs in LMBs include:

107 **Doping with Inorganic Fillers:** Incorporating inorganic fillers such as  $\text{Li}_3\text{PO}_4$ ,  $\text{Al}_2\text{O}_3$ ,  
108 or LLZTO improves ionic conductivity, mechanical strength, and stability. These fillers help  
109 reduce crystallinity in PVDF, creating more amorphous regions that facilitate lithium-ion  
110 mobility and improve electrochemical performance.

111 **Blending with Organic Fillers:** Organic additives like poly(ethylene oxide) (PEO) or  
112 poly(methyl methacrylate) (PMMA) can be blended with PVDF to increase flexibility, reduce  
113 brittleness, and improve interface compatibility with lithium metal anodes. Blending polymers  
114 also adjusts the mechanical properties, enhancing stability during battery cycling.

115 **Inorganic/Organic Composite Fillers:** A combined approach using both inorganic and  
116 organic fillers can yield synergistic benefits, where inorganic components contribute to thermal  
117 stability and ionic conductivity, while organic additives enhance flexibility and interfacial  
118 contact with electrodes.

119 **Chemical Modification of PVDF:** Chemical modifications such as grafting and  
120 functionalizing PVDF with ion-conducting groups can increase its ionic conductivity by  
121 introducing additional lithium-ion conduction pathways and lowering the glass transition



122 temperature.

123 These modification strategies, outlined in **Scheme 1**, facilitate the design of PVDF-based  
124 SSEs that meet the specific requirements of high-performance LMBs. **Table 1** summarizes the  
125 synthesis methods, compositions, and electrochemical properties of various PVDF-based SSEs  
126 tailored for LMB applications. By systematically exploring and combining these approaches,  
127 PVDF-based electrolytes can achieve the high stability, flexibility, and ionic conductivity  
128 necessary for advanced LMB technologies.

## 129 **2.1 Doping with Inorganic Fillers**

130 One of the most common enhancement strategies for PVDF-based solid-state electrolytes  
131 (SSEs) is doping with inorganic fillers. These fillers typically come in three morphological  
132 forms: zero-dimensional (0D) nanoparticles, one-dimensional (1D) nanowires, and two-  
133 dimensional (2D) nanosheets. These active fillers act as ion carriers and participate in lithium-  
134 ion ( $\text{Li}^+$ ) conduction, promoting efficient ion transfer and enhancing the electrolyte's ionic  
135 conductivity. Additionally, the free volume spaces generated at the interfaces between ceramic  
136 fillers and the PVDF matrix provide additional ion transport pathways. Consequently,  
137 introducing active fillers to boost the ionic conductivity of PVDF-based SSEs has gained  
138 substantial interest in recent years.

139 For instance, Nan et al. developed composite solid electrolytes (CSEs) with garnet-type  
140  $\text{Li}_{6.75}\text{La}_3\text{Zr}_{1.75}\text{Ta}_{0.25}\text{O}_{12}$  (LLZTO) nanoparticles as active fillers.<sup>39</sup> The La atoms in LLZTO  
141 interact with nitrogen atoms and C=O groups from the solvent N,N-dimethylformamide (DMF),  
142 creating electron-enriched nitrogen atoms that act as Lewis bases, leading to the  
143 dehydrofluorination of PVDF. This interaction between PVDF, lithium salt, and LLZTO  
144 enhances the flexible electrolyte's performance, resulting in a high ionic conductivity of  
145 approximately  $0.5 \text{ mS} \cdot \text{cm}^{-1}$  at  $25^\circ\text{C}$ . In a similar study, Liu et al. fabricated flexible CSEs using  
146 a PVDF matrix with lithium salt (LiTFSI), DMF, and NASICON-type  $\text{Li}_{1.3}\text{Al}_{0.3}\text{Ti}_{1.7}(\text{PO}_4)_3$   
147 (LATP) ceramic nanoparticles as fillers.<sup>40</sup> DMF facilitates lithium salt dissociation and forms  
148 lithium-rich complexes  $[\text{Li}(\text{DMF})_n\text{TFSI}]$  with  $\text{Li}^+$ , which exhibit ionic liquid-like  
149 characteristics that improve conductivity. This design yielded a LATP-PVDF/Li CSE with a  
150 high ionic conductivity of  $0.244 \text{ mS} \cdot \text{cm}^{-1}$  and an electrochemical stability window of up to 4.8





151 V (vs Li<sup>+</sup>/Li).

152 However, the thickness and limited mechanical strength of PVDF-based SSEs can restrict  
153 their practical applications. To address this, Ma et al. developed an ultrathin PVDF-based SSE  
154 by integrating a 7 μm polyethylene (PE) separator and SiO<sub>2</sub> nanoparticles with silicon hydroxyl  
155 (Si-OH) groups<sup>41</sup>. This composite, known as PPSE, achieved a total thickness of only 20 μm  
156 and exhibited ultra-high mechanical strength (64 MPa). The nano-SiO<sub>2</sub> particles anchored  
157 DMF molecules, enhancing ion conductivity in PVDF and preventing side reactions with  
158 lithium metal. This modification increased the ionic conductivity to 0.48 mS·cm<sup>-1</sup>, reduced  
159 activation energy (0.19 eV), and achieved a high lithium transference number (0.59).

160 Introducing functional fillers with ferroelectric or dielectric properties has also proven  
161 effective in improving PVDF-based SSEs. For instance, Kang et al. utilized dielectric NaNbO<sub>3</sub>  
162 nanoparticles in a PVDF-based SSE (PNNO-5), which induced the formation of a high-  
163 dielectric β-phase in PVDF (**Figure 1a**).<sup>42</sup> This phase enhances Li<sup>+</sup> coordination with FSI<sup>-</sup>  
164 anions due to polarized F atoms, which aid in abundant and mobile Li<sup>+</sup> ion formation (**Figure**  
165 **1b-d**). The PNNO-5 SSE achieved a high ionic conductivity of 0.556 mS·cm<sup>-1</sup>, with a  
166 decreased ion migration activation energy of 0.22 eV, as compared to 0.33 eV in unmodified  
167 PVDF SSEs (**Figure 1e**). This configuration allowed a LiNi<sub>0.8</sub>Mn<sub>0.1</sub>Co<sub>0.1</sub>O<sub>2</sub>  
168 (NCM811)/PNNO-5/Li cell to retain 67.7% capacity over 1500 cycles at 1 C and demonstrated  
169 a high initial capacity of 177.2 mAh·g<sup>-1</sup> with 95% retention over 100 cycles at 0.5 C (**Figure**  
170 **1f**).

171 Li et al. also introduced ferroelectric BiFeO<sub>3</sub> nanoparticles to modify PVDF-based SSEs,  
172 which helped distribute the electric field more uniformly at the electrolyte/electrode interface,  
173 resulting in uniform Li deposition.<sup>43</sup> The transference number of Li<sup>+</sup> increased from 0.18 to  
174 0.35 compared to pure PVDF, enhancing overall battery performance. The BiFeO<sub>3</sub> particles'  
175 spontaneous polarization along the [111] direction generates dipoles that interact  
176 electrostatically with TFSI<sup>-</sup> anions (**Figure 1g**), further dissociating LiTFSI and reducing the  
177 migration resistance of [Li(DMF)<sub>x</sub>]<sup>+</sup> complexes. The assembled Li/NCM811 full cells showed  
178 an excellent performance, which a high coulombic efficiency of 99% and a capacity retention  
179 of 89% achieved after 400 cycles (**Figure 1h**).

180 Compared to granular fillers, ceramic nanowires can substantially enhance the



181 conductivity of SSEs by creating continuous pathways that facilitate lithium-ion transport. The  
182 interconnected nanowire network also improves the electrolyte's mechanical strength, thus  
183 enhancing battery stability and safety.<sup>44</sup> For instance, Su and colleagues developed a CSE with  
184  $\text{Li}_{0.35}\text{La}_{0.55}\text{TiO}_3$  nanofibers and PVDF/LiTFSI, achieving an ionic conductivity of  $0.53$   
185  $\text{mS}\cdot\text{cm}^{-1}$  at room temperature and a voltage window up to  $5.1$  V.<sup>45</sup> Shi et al. synthesized  
186  $\text{BaTiO}_3\text{-Li}_{0.33}\text{La}_{0.56}\text{TiO}_{3-x}$  (BTO-LLTO) nanowires with a heterojunction structure through  
187 electrospinning, followed by calcination at  $1000^\circ\text{C}$ .<sup>46</sup> Introducing these nanowires into a PVDF  
188 matrix yielded a PVDF-based CSE (PVBL) with high ionic conductivity ( $0.82$   $\text{mS}\cdot\text{cm}^{-1}$ ) and  
189 lithium transference number ( $0.57$ ) (**Figure 2a-c**). The PVBL exhibited stable cycling for over  
190 1900 hours at  $0.1$   $\text{mA}\cdot\text{cm}^{-2}$  and  $0.1$   $\text{mAh}\cdot\text{cm}^{-2}$  in a symmetrical cell (**Figure 2d**) and achieved  
191 a capacity retention of 70% after 1000 cycles in an NCM811/PVBL/Li battery (**Figure 2e**).

192 In another study, He et al. incorporated g- $\text{C}_3\text{N}_4$  nanosheets (GCNs) into a PVDF-based  
193 SSE, achieving high ionic conductivity of  $0.69$   $\text{mS}\cdot\text{cm}^{-1}$ .<sup>47</sup> During cycling, GCNs react with  
194 lithium metal to form a  $\text{Li}_3\text{N}$ -enriched SEI layer, significantly reducing side reactions and  
195 ensuring rapid charge transfer. The GCNs' adsorption capacity for residual DMF further  
196 improves electrochemical stability, enabling the Li symmetrical cell to cycle steadily for 2200  
197 hours at  $0.1$   $\text{mA}\cdot\text{cm}^{-2}$  and  $0.1$   $\text{mAh}\cdot\text{cm}^{-2}$ . Additionally, the NCM811 cathode-based LMBs  
198 exhibited a high discharge capacity of  $108$   $\text{mAh}\cdot\text{g}^{-1}$  at 5 C and excellent cycling stability over  
199 1700 cycles at 1 C.

200 In summary, doping PVDF-based SSEs with various inorganic fillers - ranging from 0D  
201 nanoparticles to 1D nanowires and 2D nanosheets - enhances their electrochemical properties  
202 by increasing ionic conductivity, mechanical strength, and stability, facilitating promising  
203 applications in high-performance lithium metal batteries.

## 204 2.2 Blending with Organic Fillers

205 PVDF-based SSEs are often prepared by solution casting using DMF as a solvent, which  
206 results in the formation of a  $[\text{DMF-Li}^+]$  complex that improves  $\text{Li}^+$  transport. However, residual  
207 DMF can react with lithium metal over time, compromising the interface between the PVDF-  
208 based SSE and Li anode. To address this, Nan et al. introduced propylene carbonate (PC) into  
209 PVDF-based SSEs to stabilize the interface between the SSE and Li anode by controlling the





210 solvation structure.<sup>48</sup> PC accelerates the dissociation of lithium oxalate difluoroborate (LiODFB),  
211 forming a robust interfacial layer of "lithium propylene decarbonate (LPDC)-B-O" oligomers.  
212 This dense, uniform layer enhances contact and suppresses continuous reactions between  
213 residual DMF and the Li anode, achieving a high ionic conductivity of  $1.18 \text{ mS}\cdot\text{cm}^{-1}$ . The  
214 resulting LiCoO<sub>2</sub>/Li full batteries deliver  $139.2 \text{ mAh}\cdot\text{g}^{-1}$ , retaining 84% of capacity after 300  
215 cycles at 0.1C.

216 To further stabilize the interface, Zhang et al. incorporated isosorbide mononitrate (ISMN),  
217 a functional additive with a non-resonant structure (O<sub>2</sub>-N-O-), into PVDF-based SSEs to  
218 create a stable N-rich solid electrolyte interface, reducing Li dendrite formation and side  
219 reactions (**Figure 3a**).<sup>49</sup> ISMN, when added to PVDF-based SSEs, forms a stable interface  
220 upon lithium stripping/plating by cleaving the N-O bond in its non-resonant structure, yielding  
221 a nitrogen-rich layer that enhances ultra-stable flexible SSLMBs. The Li/Li symmetric cell  
222 achieved stable Li stripping/plating cycling for over 5000 hours at a current density of 0.2  
223 mA·cm<sup>-2</sup> and capacity of  $1.0 \text{ mAh}\cdot\text{cm}^{-2}$ . Additionally, the Li|LiFePO<sub>4</sub> cell exhibited an initial  
224 discharge capacity of  $154.0 \text{ mAh}\cdot\text{g}^{-1}$ , with a capacity retention of 88.9% after 500 cycles at 0.5  
225 C. The flexible NCM622/Li pouch cell maintained a high discharge capacity retention of 97.2%  
226 over 100 cycles at 0.5 C.

227 Moreover, Nan et al. developed a PVDF-based SSE with 2-acrylamido-2-methylpropane  
228 sulfonic acid (AMPS) as an additive to enhance Li<sup>+</sup> conduction by reducing the crystallinity of  
229 PVDF and immobilizing anions.<sup>50</sup> AMPS induces the formation of a LiF/Li<sub>2</sub>S<sub>x</sub>/Li<sub>2</sub>SO<sub>3</sub>/Li<sub>3</sub>N-  
230 rich interface at the Li anode, suppressing dendrite growth (**Figure 3b-d**). The resulting AMPS-  
231 PVDF polymer electrolyte (AP-PE) enables symmetric cells to cycle stably for 2100 hours at  
232  $0.1 \text{ mA}\cdot\text{cm}^{-2}$  and  $0.1 \text{ mAh}\cdot\text{cm}^{-2}$ . After 500 hours of cycling, the Li anode in these symmetric  
233 cells exhibited a clean surface with no dendrite formation (**Figure 3e**). The Li/AP-PE/LFP cell  
234 demonstrated stable cycling performance, retaining 90.8% of its capacity after 200 cycles at  
235 0.5 C (**Figure 3e-g**).

236 By blending PVDF-based SSEs with various organic fillers, researchers have significantly  
237 enhanced ionic conductivity, interface stability, and cycling performance, making these  
238 electrolytes viable candidates for high-performance, long-lasting LMBs.



### 239 2.3 Inorganic/Organic Composite Fillers

240 In PVDF-based SSEs, porous structures can lead to disordered ion flux and reduced  
241 mechanical strength, resulting in non-uniform lithium deposition and promoting lithium  
242 dendrite growth (**Figure 4a**). To address this, Ma et al. designed a composite filler by  
243 incorporating interconnected metal-organic framework (MOF)-coated heat-treated  
244 polyacrylonitrile (h-PAN@MOF) fiber networks into a PVDF matrix, creating composite SSEs  
245 termed PPM (**Figure 4b**). The MOF (UIO-66NH<sub>2</sub>) particles on the PAN fibers interact strongly  
246 with the C=O groups of DMF molecules, weakening the Li<sup>+</sup>-O bond strength in DMF and  
247 facilitating Li<sup>+</sup> transport along the h-PAN@MOF networks. This design achieved a high ionic  
248 conductivity of 1.03 mS·cm<sup>-1</sup> (**Figure 4a**).

249 The h-PAN@MOF network also imparts high mechanical strength (20.84 MPa) to the  
250 electrolyte, effectively inhibiting lithium dendrite growth. The adsorption energy of the C=O  
251 group in DMF on the MOF crystal (-1.11 eV) is three times greater than that on the PVDF  
252 chains (-0.35 eV). This strong adsorptive interaction between DMF and MOF realigns solvent  
253 molecules around the h-PAN@MOF networks, significantly reducing DMF decomposition at  
254 the PPM electrolyte/lithium metal interface.

255 Solid-state nuclear magnetic resonance (ss-NMR) spectroscopy of the <sup>7</sup>Li and <sup>19</sup>F spectra  
256 was conducted to examine the interactions between FSI-Li<sup>+</sup> and DMF-Li<sup>+</sup> complexes. An  
257 upfield shift in the <sup>7</sup>Li spectrum indicates an enhanced shielding effect of lithium nuclei in the  
258 PPM electrolyte, suggesting tighter coordination with surrounding ligands (**Figure 4c**).  
259 Changes in chemical shifts in the <sup>19</sup>F spectra of FSI also indicate a weakened DMF-Li<sup>+</sup>  
260 interaction and stronger FSI-Li<sup>+</sup> coordination (**Figure 4d**). The combined effects of h-PAN and  
261 MOF establish a competitive Li<sup>+</sup> coordination environment and alter solvation structures to  
262 promote rapid, linear Li<sup>+</sup> transport. This synergy enhances interfacial stability with electrodes.

263 As a result, the Li|PPM|Li battery demonstrated stable voltage hysteresis over 3200 hours  
264 at a current density of 0.1 mA·cm<sup>-2</sup> and a capacity of 0.1 mAh·cm<sup>-2</sup> (**Figure 4e**). Additionally,  
265 the Li|PPM|NCM811 battery retained 61.9% of its capacity over 1400 cycles at 2C (**Figure**  
266 **4f**). This promising performance highlights the effectiveness of inorganic/organic composite  
267 fillers in enhancing the stability and ionic conductivity of PVDF-based SSEs in lithium metal



268 batteries.

View Article Online  
DOI: 10.1039/D4NR04583A

## 269 2.4 Chemical Modification of PVDF

270 Beyond doping fillers and blending with polymers, direct modification of PVDF is an  
271 effective method to enhance the performance of PVDF-based SSEs. For example, Zeng et al.  
272 modified PVDF by introducing –OH groups into the PVDF chain segments<sup>51</sup>. By applying  
273 molecular anchoring principles, the typically disordered DMSO molecules within PVDF align  
274 through hydrogen bonding, creating an efficient pathway for rapid Li<sup>+</sup> transport. The resulting  
275 LFP|PVDF–OH|Li battery achieved an initial capacity of 145.9 mAh·g<sup>-1</sup> at 0.5C, with a  
276 capacity retention of 85.4% after 1000 cycles. Additionally, the PVDF–OH SSE in an LFP|Li  
277 pouch battery delivered an initial capacity of 124.47 mAh·g<sup>-1</sup>, retaining 98% of its capacity  
278 after 200 cycles at 0.5C.

279 In another advancement, Huang et al. demonstrated that Li<sup>+</sup> can transport through the  
280 crystalline phase of PVDF by incorporating dipolar defects into the crystals.<sup>52</sup> By adding  
281 trifluoroethylene (CHF<sub>3</sub>) and chlorofluoroethylene (CH<sub>2</sub>FCI) as dipolar defects into VDF  
282 crystals, they triggered rapid Li<sup>+</sup> movement through ion–dipole interactions. These defects  
283 expanded the interchain distance in PVDF from 4.39 to 4.83 Å, facilitating –CH<sub>2</sub>CF<sub>2</sub> dipole  
284 vibrations at room temperature and supporting Li<sup>+</sup> migration through ion-dipole interactions,  
285 thereby transforming PVDF into a fast ion conductor (**Figure 5a**). As a result, the defective  
286 PVDF (d-PVDF) SSE achieved a high ionic conductivity of 0.78 mS·cm<sup>-1</sup> and a lithium-ion  
287 transference number (tLi<sup>+</sup>) of 0.57 (**Figure 5d**).

288 Further analysis with displacement-electric field (D–E) measurements showed that d-  
289 PVDF, unlike ferroelectric (FE) PVDF, exhibited a slim hysteresis loop, indicating a significant  
290 reduction in coercive field from 67.3 to 10.7 MV·m<sup>-1</sup> (**Figure 5b**). This observation confirmed  
291 the presence of –CHF<sub>3</sub> and –CH<sub>2</sub>FCI dipolar defects in the VDF crystals, which promote Li<sup>+</sup>  
292 integration within the crystals, transforming defective d-PVDF crystals into single-ion  
293 conductors (**Figure 5c**). The Li/d-PVDF/Li symmetrical cell demonstrated an extended  
294 lifespan of 11,000 hours (450 days) at 0.05 mA·cm<sup>-2</sup> (**Figure 5e**). Furthermore, NCM811/d-  
295 PVDF/Li batteries exhibited excellent capacity retention of 94.9% after 300 cycles at 1C.

296 These findings underscore the potential of modifying PVDF to create fast ion-conducting



297 pathways, achieving significant improvements in ionic conductivity, lithium-ion transference,  
298 and overall stability in PVDF-based SSEs for advanced lithium metal batteries.

## 299 2.5 Other Strategies

300 Beyond filler addition, constructing composite solid electrolytes (CSEs) with a ceramic  
301 body and a 3D-engineered scaffold infiltrated with a conductive polymer offers significant  
302 potential. This approach provides enhanced ionic transport, electrochemical stability, low  
303 interfacial resistance, and high mechanical strength. Wang et al. developed a conductive CSE  
304 featuring a cubic  $\text{Li}_{6.1}\text{Al}_{0.3}\text{La}_3\text{Zr}_2\text{O}_{12}$  (LLZO) porous framework embedded in PVDF,  
305 forming a continuous 3D structure (**Figure 6a**).<sup>53</sup> The formation of La–N and La–F bonds  
306 between the ceramic and polymer matrix aids Li salt dissociation, enabling efficient ion  
307 transport. These interactions led to a high ionic conductivity of  $0.437 \text{ mS}\cdot\text{cm}^{-1}$  and a lithium-  
308 ion transference number ( $t_{\text{Li}^+}$ ) of 0.72 at 25°C.

309 The ceramic skeleton creates a 3D conductive network with micron-sized pores that allow  
310 solubilized SSEs to permeate (**Figure 6b**). The resulting SSE has high porosity (45.74%) and  
311 a wide voltage window (5.08 V), making it compatible with high-voltage cathodes. The  
312 ceramic-based SSE, with a high ceramic-mass composition (93%), provides robust mechanical  
313 support that suppresses lithium dendrite formation, while the porous LLZO framework allows  
314 for substantial PVDF-LiTFSI loading (**Figure 6c**).

315 When used in LiNCM622/ceramic-based SSE/Li full solid-state lithium metal batteries  
316 (SSLMBs), the CSE demonstrated stable cycling over 200 times within a voltage range of 3 to  
317 4.8 V, maintaining a high Coulombic efficiency of 99.76% at 0.2C (**Figure 6d**). After 200  
318 cycles, the interfacial zone between the cathode and CSE remained intact, with no delamination  
319 or cracking. Additionally, an  $\text{F}^-$  and N-rich interface formed between the cathode and ceramic-  
320 based CSE, enhancing stability and performance (**Figure 6e**). This 3D scaffold approach  
321 highlights the potential for creating stable, high-performance PVDF-based SSEs suitable for  
322 high-voltage and long-cycle SSLMB applications.

## 323 3. Conclusion and Perspective

324 In summary, this review has highlighted the applications of PVDF-based SSEs in lithium



325 metal anodes, covering strategies such as doping with inorganic fillers, blending with organic  
326 fillers, incorporating inorganic/organic composite fillers, modifying PVDF, and other  
327 approaches. Related fabrication methods, micro- and nanostructures, and electrochemical  
328 performance improvements have been systematically reviewed. These strategies have  
329 significantly enhanced the electrochemical performance of PVDF-based solid-state lithium  
330 metal batteries. However, several critical challenges remain for advancing PVDF-based SSEs  
331 to practical applications. Future studies may focus on the following areas:

332 **Development of Functional Materials to Modify PVDF-based SSEs.** Current research  
333 mainly focuses on PVDF-based SSEs at low current densities and room temperatures. It is  
334 essential to develop PVDF-based SSEs with high thermal and electrochemical stability that can  
335 operate under elevated temperatures and higher current rates. Additionally, most modified  
336 fillers are limited to metal oxide electrolytes within PVDF matrices. Exploration of PVDF-  
337 based SSEs with sulfide and halide electrolytes is still limited, despite the superior ionic  
338 conductivity of sulfides. Combining PVDF-based SSEs with sulfide electrolytes could  
339 potentially improve SSLMB electrochemical performance.

340 **In-depth Mechanistic Studies of PVDF-based SSEs in LMBs.** Although considerable  
341 research has been conducted on PVDF-based SSE materials, theoretical calculations and  
342 mechanistic insights remain underexplored. Establishing a comprehensive evaluation standard  
343 for PVDF-based SSEs in LMBs is crucial for future material advancements. Advanced  
344 operando techniques, such as in-situ X-ray diffraction (XRD), scanning electron microscopy  
345 (SEM), transmission electron microscopy (TEM), and nuclear magnetic resonance (NMR), are  
346 essential for real-time insights into ion transport during the charging/discharging process.  
347 Integrating theoretical calculations (e.g., DFT calculations, molecular dynamics simulations)  
348 with in-situ characterization techniques is urgently needed to understand surface and interfacial  
349 chemistry and physics changes during cycling.

350 **Development of Thin PVDF-based SSEs with High Mechanical Strength.** Current  
351 PVDF-based SSEs typically have thicknesses around 100  $\mu\text{m}$ , limiting their potential to  
352 enhance energy density. Thinner electrolytes (10–20  $\mu\text{m}$ ) are essential for achieving higher  
353 energy density in SSLMBs. At the same time, these thinner electrolytes must possess sufficient  
354 mechanical strength to prevent lithium dendrite penetration, which may require incorporating



355 inorganic materials. To support high-loading cathodes, combining cathode materials with solid  
356 electrolytes could be a viable solution.

357 **Bridging the Gap between Research and Practical Applications.** The development of  
358 300 Wh kg<sup>-1</sup> pouch cells represents a significant advancement in SSLMBs, positioning them  
359 closer to commercial viability. Pouch cells hold the potential to further elevate SSLMB energy  
360 densities to 500 Wh kg<sup>-1</sup>, which could expedite their industrialization and application in daily  
361 life. The production of PVDF-based lithium metal pouch cells has a promising future, although  
362 numerous unknown challenges still need to be addressed.

363 In conclusion, this review provides a foundational understanding and recent  
364 advancements in the design and use of PVDF-based SSEs for SSLMBs. It will inform future  
365 efforts in developing high-performance PVDF-based SSLMBs and help accelerate their  
366 practical applications.

### 367 Acknowledgements

368 Z.L. and G.X. acknowledge the support of National Key Research and Development Program  
369 of China (2022YFB3803502), National Natural Science Foundation of China (52103076), and  
370 Shanghai Rising-Star Program (24QA2700100). M.S.I. and C.C. thank the support of USDA-  
371 NIFA (Grant No. 2021-67021-33998) and Case Western Reserve University.

### 373 Reference

- 374 1. C. Dang, Y. Cao, H. Nie, W. Lang, J. Zhang, G. Xu and M. Zhu, *Nature Water*, 2024, **2**, 115-126.
- 375 2. A. Olabi and M. A. Abdelkareem, *Renewable and Sustainable Energy Reviews*, 2022, **158**, 112111.
- 376 3. Y. Pang, Y. Cao, M. Derakhshani, Y. Fang, Z. L. Wang and C. Cao, *Matter*, 2021, **4**, 116-143.
- 377 4. Y. Pang, Y. Fang, J. Su, H. Wang, Y. Tan and C. Cao, *Advanced Materials Technologies*, 2023, **8**,  
378 2201246.
- 379 5. Y. Pang, Z. Huang, Y. Fang, X. Xu and C. C. Cao, *Nano Energy*, 2023, **114**, 108659.
- 380 6. X. Zhu, Z. Xu, T. Zhang, J. Zhang, Y. Guo, M. Shan, K. Wang, T. Shi, G. Cui, F. Wang, G. Xu and M.  
381 Zhu, *Advanced Functional Materials*, 2024, **34**, 2407262.
- 382 7. S. Chen, M. Zhang, P. Zou, B. Sun and S. Tao, *Energy & Environmental Science*, 2022, **15**, 1805-1839.
- 383 8. J. Xu, X. Cai, S. Cai, Y. Shao, C. Hu, S. Lu and S. Ding, *Energy & Environmental Materials*, 2023, **6**,  
384 e12450.
- 385 9. Y. Pang, Y. Cao, Y. Chu, M. Liu, K. Snyder, D. MacKenzie and C. Cao, *Advanced Functional Materials*,  
386 2020, **30**, 1906244.
- 387 10. S. Chae, S. H. Choi, N. Kim, J. Sung and J. Cho, *Angewandte Chemie International Edition*, 2020, **59**,  
388 110-135.





- 389 11. B. Liu, J.-G. Zhang and W. Xu, *Joule (Netherlands)*, 2018, **2**, 833-845.
- 390 12. B. Jagger and M. Pasta, *Joule (Netherlands)*, 2023, **7**, 2228-2244.
- 391 13. Z. X. Liu, S. H. Ha, Y. Liu, F. Wang, F. Tao, B. R. Xu, R. H. Yu, G. X. Wang, F. Z. Ren and H. X. Li,  
392 *Journal of Materials Science & Technology*, 2023, **133**, 165-182.
- 393 14. X. Yang, Q. Yin, C. Wang, K. Doyle-Davis, X. Sun and X. Li, *Progress in Materials Science*, 2023, **140**,  
394 101193.
- 395 15. J. Wang, B. Ge, H. Li, M. Yang, J. Wang, D. Liu, C. Fernandez, X. Chen and Q. Peng, *Chemical*  
396 *Engineering Journal*, 2021, **420**, 129739.
- 397 16. S. Y. Yuan, T. Y. Kong, Y. Y. Zhang, P. Dong, Y. J. Zhang, X. L. Dong, Y. G. Wang and Y. Y. Xia,  
398 *Angewandte Chemie-International Edition*, 2021, **60**, 25624-25638.
- 399 17. Z. Liu, Y. Liu, Y. Miao, G. Liu, R. Yu, K. Pan, G. Wang, X. Pang and J. Ma, *Energy and Environmental*  
400 *Material*, 2023, **6**, e12525.
- 401 18. Y. Lin, S. Huang, L. Zhong, S. Wang, D. Han, S. Ren, M. Xiao and Y. Meng, *Energy Storage Materials*,  
402 2021, **34**, 128-147.
- 403 19. F. Liang, Y. L. Sun, Y. F. Yuan, J. Huang, M. J. Hou and J. Lu, *Materials Today*, 2021, **50**, 418-441.
- 404 20. J. Wu, S. Liu, F. Han, X. Yao and C. Wang, *Advanced Materials*, 2021, **33**, 2000751.
- 405 21. P. Hagenmuller and W. Van Gool, *Solid electrolytes: general principles, characterization, materials,*  
406 *applications*, Elsevier, 2013.
- 407 22. T. Ye, L. Li and Y. Zhang, *Advanced Functional Materials*, 2020, **30**, 2000077.
- 408 23. Z. Y. Wang, L. Shen, S. G. Deng, P. Cui and X. Y. Yao, *Advanced Materials*, 2021, **33**, 2100353.
- 409 24. J. C. Bachman, S. Muy, A. Grimaud, H. H. Chang, N. Pour, S. F. Lux, O. Paschos, F. Maglia, S. Lupart,  
410 P. Lamp, L. Giordano and Y. Shao-Horn, *Chemical Reviews*, 2016, **116**, 140-162.
- 411 25. Q. Zheng, Y. Song, W. Huang, J. Yang, T. Li and Y. Xu, *Energy Storage Materials*, 2023, **63**, 103038.
- 412 26. S. Kalnaus, N. J. Dudney, A. S. Westover, E. Herbert and S. Hackney, *Science* 2023, **381**, eabg5998.
- 413 27. Y. M. Jin, Q. S. He, G. Z. Liu, Z. Gu, M. Wu, T. Y. Sun, Z. H. Zhang, L. F. Huang and X. Y. Yao,  
414 *Advanced Materials*, 2023, **35**, 2211047.
- 415 28. P. Jiang, G. Du, J. Cao, X. Zhang, C. Zou, Y. Liu and X. Lu, *Energy Technology*, 2023, **11**, 2201288.
- 416 29. Q. Zhang, D. Cao, Y. Ma, A. Natan, P. Aurora and H. Zhu, *Advanced Materials*, 2019, **31**, 1901131.
- 417 30. Z. H. Zhang, L. P. Wu, D. Zhou, W. Weng and X. Y. Yao, *Nano Letters*, 2021, **21**, 5233-5239.
- 418 31. M. L. Yang, Y. Yao, M. Y. Chang, F. L. Tian, W. R. Xie, X. L. Zhao, Y. Yu and X. Y. Yao, *Advanced*  
419 *Energy Materials*, 2023, **13**, 2300962.
- 420 32. L. Hu, X. Gao, H. Wang, Y. Song, Y. Zhu, Z. Tao, B. Yuan and R. Hu, *Small*, 2024, 2312251.
- 421 33. Z. H. Jia, Y. Liu, H. M. Li, Y. Xiong, Y. J. Miao, Z. X. Liu and F. Z. Ren, *Journal of Energy Chemistry*,  
422 2024, **92**, 548-571.
- 423 34. Y. Gong, C. Wang, M. Xin, S. Chen, P. Xu, D. Li, J. Liu, Y. Wang, H. Xie, X. Sun and Y. Liu, *Nano*  
424 *Energy*, 2023, **119**, 109054.
- 425 35. Y. Wu, Y. Li, Y. Wang, Q. Liu, Q. Chen and M. Chen, *Journal of Energy Chemistry*, 2022, **64**, 62-84.
- 426 36. F. Liu, N. A. Hashim, Y. Liu, M. M. Abed and K. Li, *Journal of membrane science*, 2011, **375**, 1-27.
- 427 37. X. Zhang, S. Wang, C. J. Xue, C. Z. Xin, Y. H. Lin, Y. Shen, L. L. Li and C. W. Nan, *Advanced Materials*,  
428 2019, **31**, 1806082.
- 429 38. X. Zhang, S. Wang, C. Xue, C. Xin, Y. Lin, Y. Shen, L. Li and C.-W. Nan, *Advanced Materials*, 2020,  
430 **32**, 2000026.
- 431 39. X. Zhang, T. Liu, S. Zhang, X. Huang, B. Xu, Y. Lin, B. Xu, L. Li, C.-W. Nan and Y. Shen, *Journal of*  
432 *the American Chemical Society*, 2017, **139**, 13779-13785.



- 433 40. L. Liu, D. C. Zhang, J. W. Zhao, J. D. Shen, F. K. Li, Y. Yang, Z. B. Liu, W. X. He, W. M. Zhao and J. Liu, *Acs Applied Energy Materials*, 2022, **5**, 2484-2494. View Article Online  
DOI: 10.1039/D1NR04583A
- 434
- 435 41. K. Hashimoto, T. Shiwaku, H. Aoki, H. Yokoyama, K. Mayumi and K. Ito, *Science advances*, 2023, **9**, eadi8505.
- 436
- 437 42. X. An, Y. Liu, K. Yang, J. Mi, J. Ma, D. Zhang, L. Chen, X. Liu, S. Guo, Y. Li, Y. Ma, M. Liu, Y.-B. He and F. Kang, *Advanced Materials*, 2024, **36**, 2311195.
- 438
- 439 43. Y. Wu, H. Zhang, Y. Xu, Z. Tang and Z. Li, *Journal of Materials Chemistry A*, 2024, **12**, 20403-20413.
- 440 44. Q. Zhu, T. Zhang, X. Zhu, J. Zhang, M. Shan, Z. Hu, G. Xu and M. Zhu, *Energy Materials*, 2024, **4**, 400016.
- 441
- 442 45. B. Li, Q. Su, L. Yu, D. Wang, S. Ding, M. Zhang, G. Du and B. Xu, *Acs Applied Materials & Interfaces*, 2019, **11**, 42206-42213.
- 443
- 444 46. P. R. Shi, J. B. Ma, M. Liu, S. K. Guo, Y. F. Huang, S. W. Wang, L. H. Zhang, L. K. Chen, K. Yang, X. T. Liu, Y. H. Li, X. F. An, D. F. Zhang, X. Cheng, Q. D. Li, W. Lv, G. M. Zhong, Y. B. He and F. Y. Kang, *Nature Nanotechnology*, 2023, **18**, 602.
- 445
- 446
- 447 47. L. K. Chen, T. Gu, J. B. Ma, K. Yang, P. R. Shi, J. Biao, J. S. Mi, M. Liu, W. Lv and Y. B. He, *Nano Energy*, 2022, **100**, 107470.
- 448
- 449 48. Y. Liang, J. Zhang, S. Guan, K. Wen, C. Guo, Y.-H. Wu, H. Yuan, S. Liu, Y. Qi, W. Mo, X. Zhang and C. W. Nan, *Journal of Materiomics*, 2024, **10**, 880-888.
- 450
- 451 49. S. Zhang, H. Liu, Z. Liu, Y. Zhao, J. Yan, Y. Zhang, F. Liu, Q. Liu, C. Liu, G. Sun, Z. Wang, J. Yang and Y. Ren, *Advanced Functional Materials*, 2024, **34**, 2401377.
- 452
- 453 50. S. Guan, K. Wen, Y. Liang, C. Xue, S. Liu, J. Yu, Z. Zhang, X. Wu, H. Yuan, Z. Lin, H. Yu, L. Li and C.-W. Nan, *Journal of Materials Chemistry A*, 2022, **10**, 24269-24279.
- 454
- 455 51. Q. Zeng, D. Zhu, J. Shan, Q. Gao, J. Xu, Q. Xu, P. Shi and Y. Min, *Chemical Engineering Journal*, 2024, **486**, 150189.
- 456
- 457 52. C. Dai, M. Weng, B. Cai, J. Liu, S. Guo, H. Xu, L. Yao, F. J. Stadler, Z. M. Li and Y. F. Huang, *Energy & Environmental Science*, 2024, **17**, 8243-8253.
- 458
- 459 53. S. Wang, S. Bessette, R. Gauvin and G. P. Demopoulos, *Cell Reports Physical Science*, 2024, **5**, 102213.
- 460 54. P. R. Shi, J. B. Ma, M. Liu, S. K. Guo, Y. F. Huang, S. W. Wang, L. H. Zhang, L. K. Chen, K. Yang, X. T. Liu, Y. H. Li, X. F. An, D. F. Zhang, X. Cheng, Q. D. Li, W. Lv, G. M. Zhong, Y. B. He and F. Y. Kang, *Nature Nanotechnology*, 2023, **18**, 602-+.
- 461
- 462
- 463 55. T. Pareek, S. Dwivedi, S. A. Ahmad, M. Badole and S. Kumar, *Journal of Alloys and Compounds*, 2020, **824**, 153991.
- 464
- 465 56. X. Bai, G. Zhao, G. Yang, M. Wang, J. Zhang and N. Zhang, *Energy Storage Materials*, 2023, **63**, 103041.
- 466 57. X. Song, T. Zhang, S. Huang, J. Mi, Y. Zhang, J. Travas-Sejdic, A. P. Turner, W. Gao and P. Cao, *Journal of Power Sources*, 2023, **564**, 232849.
- 467
- 468 58. F. Liu, L. Gao, Z. Zhang, L. Zhang, N. Deng, Y. Zhao and W. Kang, *Energy Storage Materials*, 2024, **64**, 103072.
- 469
- 470 59. W. Yang, Y. Liu, X. Sun, Z. He, P. He and H. Zhou, *Angewandte Chemie-International Edition*, 2024, **63**, e202401428
- 471
- 472 60. P. Yao, B. Zhu, H. Zhai, X. Liao, Y. Zhu, W. Xu, Q. Cheng, C. Jayyosi, Z. Li, J. Zhu, K. M. Myers, X. Chen and Y. Yang, *Nano Letters*, 2018, **18**, 6113-6120.
- 473
- 474 61. T. S. Feng, Y. B. Hu, L. Xu, J. Q. Huang, S. B. Hu, L. F. Zhang and L. L. Luo, *Materials Today Energy*, 2022, **28**, 101062.
- 475
- 476 62. S. Lv, X. He, Z. Ji, S. Yang, L. Feng, X. Fu, W. Yang and Y. Wang, *Advanced Energy Materials*, 2023,

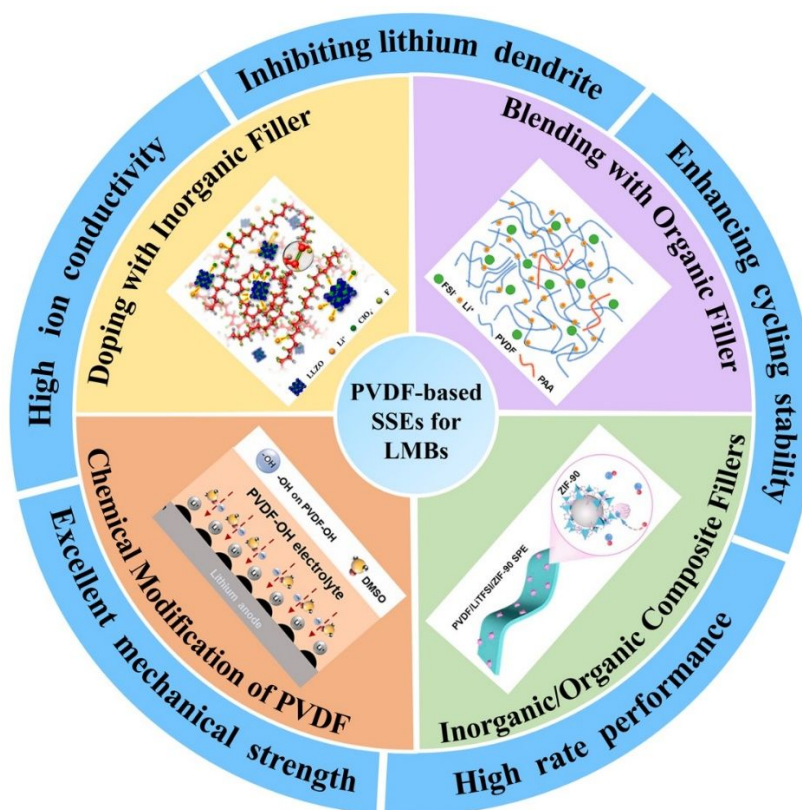


- 477 **13**, 2302711. View Article Online  
DOI: 10.1039/D4NR04583A
- 478 63. R. Orenstein, Z. Li, M. Dirican, H. Cheng, L. Chang, M. Yanilmaz, C. Yan and X. Zhang, *Acs Applied*
- 479 *Materials & Interfaces*, 2024, **16**, 33428-33438.
- 480 64. L. K. Chen, T. Gu, J. B. Ma, K. Yang, P. R. Shi, J. Biao, J. S. Mi, M. Liu, W. Lv and Y. B. He, *Nano*
- 481 *Energy*, 2022, **100**.
- 482 65. Y. Zhao, Y. Qin, X. Da, X. Weng, Y. Gao, G. Gao, Y. Su and S. Ding, *Chemsuschem*, 2022, **15**,
- 483 e202201554.
- 484 66. C. Xue, X. Zhang, S. Wang, L. Li and C.-W. Nan, *Acs Applied Materials & Interfaces*, 2020, **12**, 24837-
- 485 24844.
- 486 67. Y. Hu, L. Liu, J. Zhao, D. Zhang, J. Shen, F. Li, Y. Yang, Z. Liu, W. He, W. Zhao and J. Liu, *Batteries*,
- 487 2023, **9**, 322.
- 488 68. X. Y. Hu, K. L. Liu, S. J. Zhang, G. S. Shao, S. R. P. Silva and P. Zhang, *Nano Research*, 2023, **17**,
- 489 2824-2835.
- 490 69. X. Li, Y. Wang, Q. Zhou, H. Kuai, C. Ji and X. Xiong, *Journal of Materials Chemistry A*, 2024, **12**,
- 491 7645-7653.
- 492 70. L. Yang, Y. Mu, L. Zou, C. Li, Y. Feng, Y. Chu, D. Zuo, S. Das, L. Wei, Q. Zhang, J. Wan and L. Zeng,
- 493 *Nano letters*, 2024, **24**, 13162-13171.
- 494 71. Y. T. Ma, Y. Qiu, K. Yang, S. Lv, Y. H. Li, X. F. An, G. Y. Xiao, Z. Han, Y. T. Ma, L. K. Chen, D. F.
- 495 Zhang, W. Lv, Y. Tian, T. Z. Hou, M. Liu, Z. Zhou, F. Y. Kang and Y. B. He, *Energy & Environmental*
- 496 *Science*, 2024, **17**, 8274-8283.
- 497 72. K. Fan, X. Lai, Z. Zhang, L. Chai, Q. Yang, G. He, S. Liu, L. Sun, Y. Zhao, Z. Hu and L. Wang, *Journal*
- 498 *of Power Sources*, 2023, **580**, 233342.
- 499 73. Y. Liang, L. Dong, S. Zhong, B. Yuan, Y. Dong, Y. Liu, C. Yang, D. Tang, J. Han and W. He, *Materials*
- 500 *Today Physics*, 2021, **21**, 100554.
- 501 74. B. Cheng, P. Du, J. Xiao, X. Zhan and L. Zhu, *Acs Applied Materials & Interfaces*, 2024, **16**, 31648-
- 502 31656.
- 503 75. Y. F. Huang, T. Gu, G. Rui, P. Shi, W. Fu, L. Chen, X. Liu, J. Zeng, B. Kang, Z. Yan, F. J. Stadler, L.
- 504 Zhu, F. Kang and Y. B. He, *Energy & Environmental Science*, 2021, **14**, 6021-6029.
- 505
- 506



507 **Figures and Figure Captions**

508



509

510 **Scheme 1.** Design Strategies and Properties of PVDF-based Flexible Electrolytes for High-

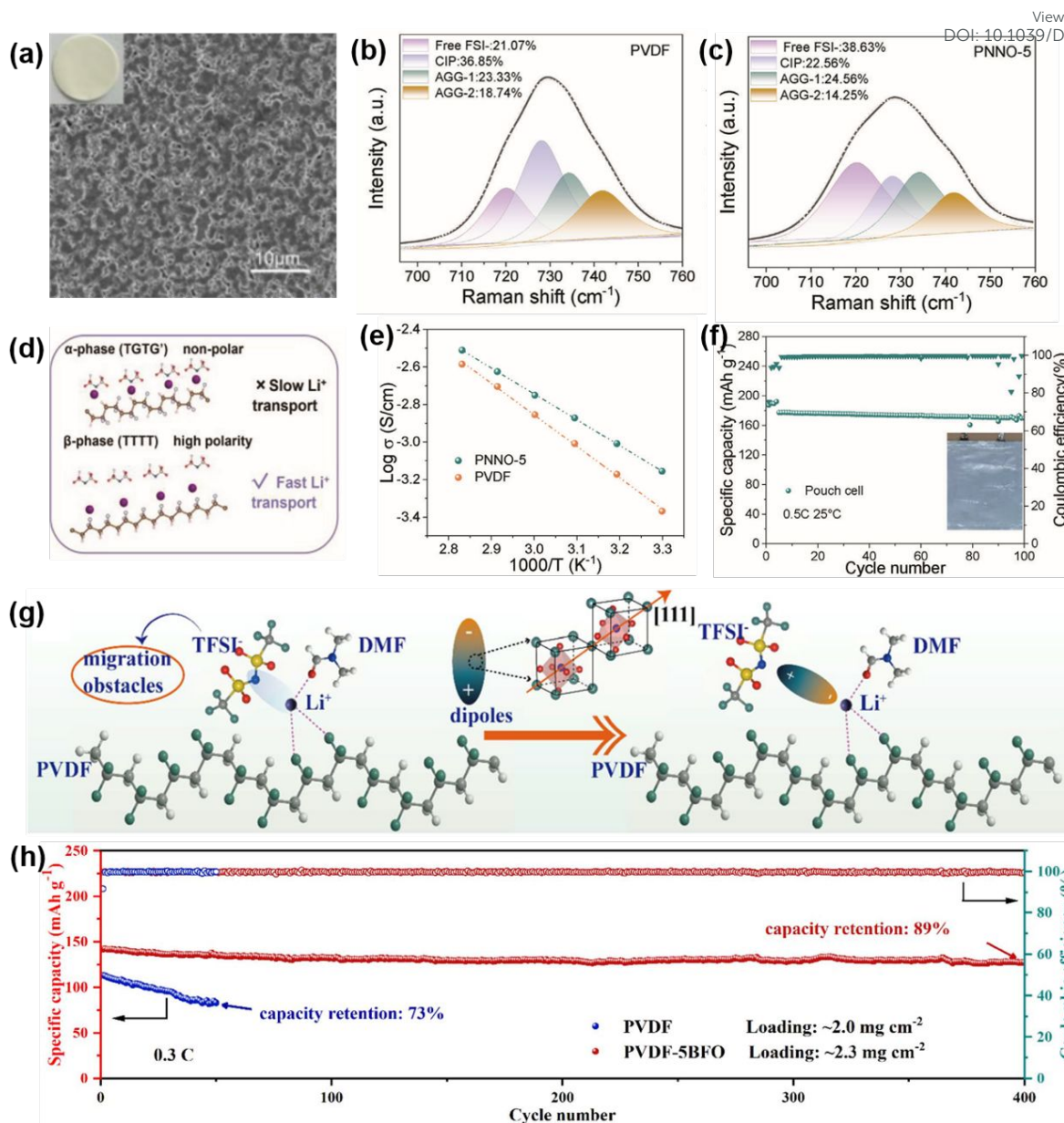
511 Performance All Solid-State Lithium Metal Batteries (LMBs).

512

513



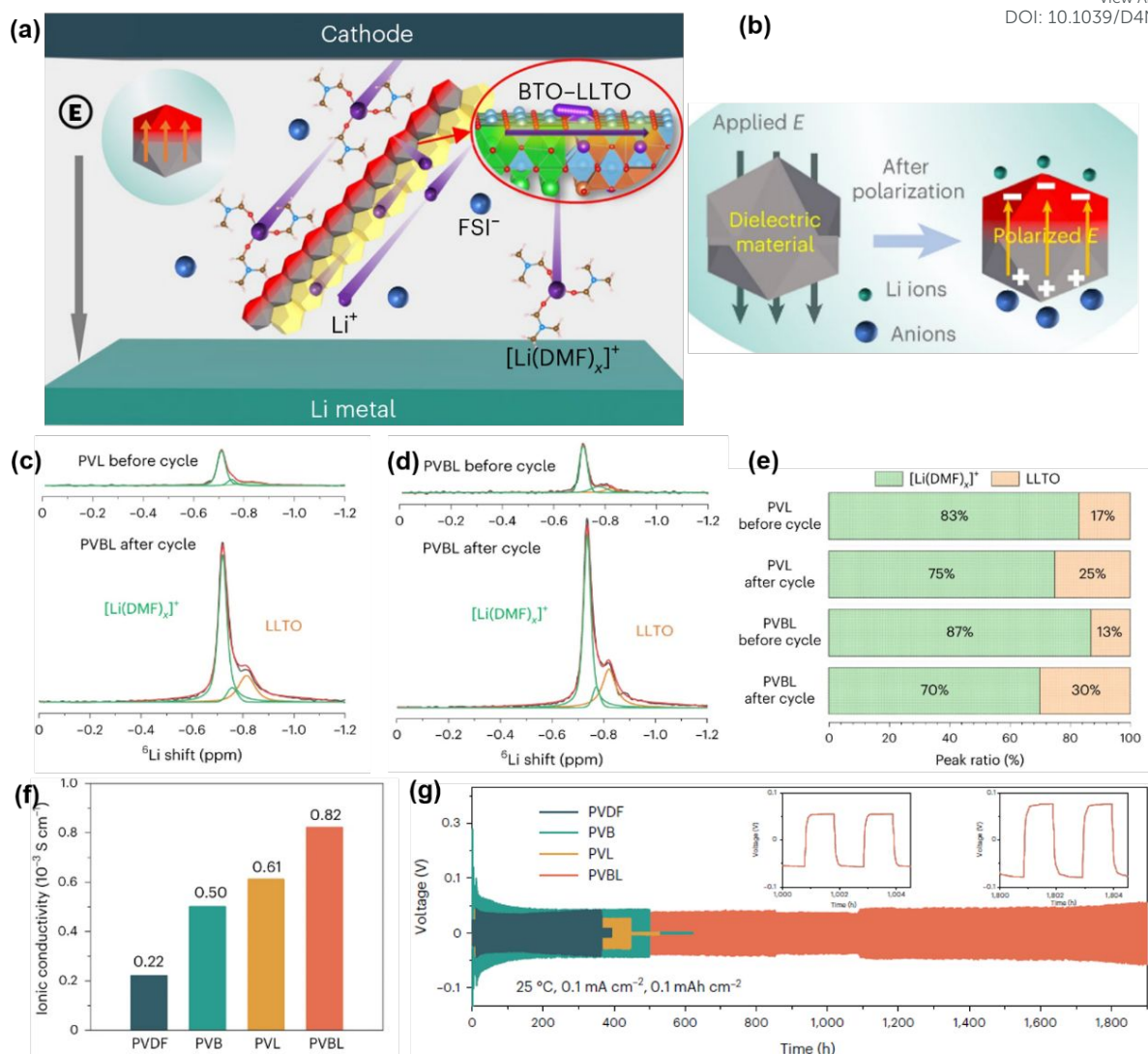




514

515 **Figure 1. Introducing functional fillers with ferroelectric or dielectric properties to**  
 516 **improve PVDF-based SSEs. (a)** Surface SEM images and optical photographs of PNNO-5.  
 517 **(b-c)** Raman spectra of PVDF and PNNO-5. **(d)** Schematic illustration showing Li salt  
 518 dissociation facilitated by the  $\beta$ -phase of PVDF. **(e)** Arrhenius plots comparing ionic  
 519 conductivity of PVDF and PNNO-5 electrolytes. **(f)** Cycling performance of NCM811/PNNO-  
 520 5/Li pouch cell. Reproduced with permission.<sup>42</sup> Copyright 2024, Advanced Materials. **(g)**  
 521 Schematic illustration of the dipole effect on the conduction mechanism. **(h)** Cycling  
 522 performance of Li/NCM811 batteries. Reproduced with permission.<sup>43</sup> Copyright 2024, Journal  
 523 of Materials Chemistry A.





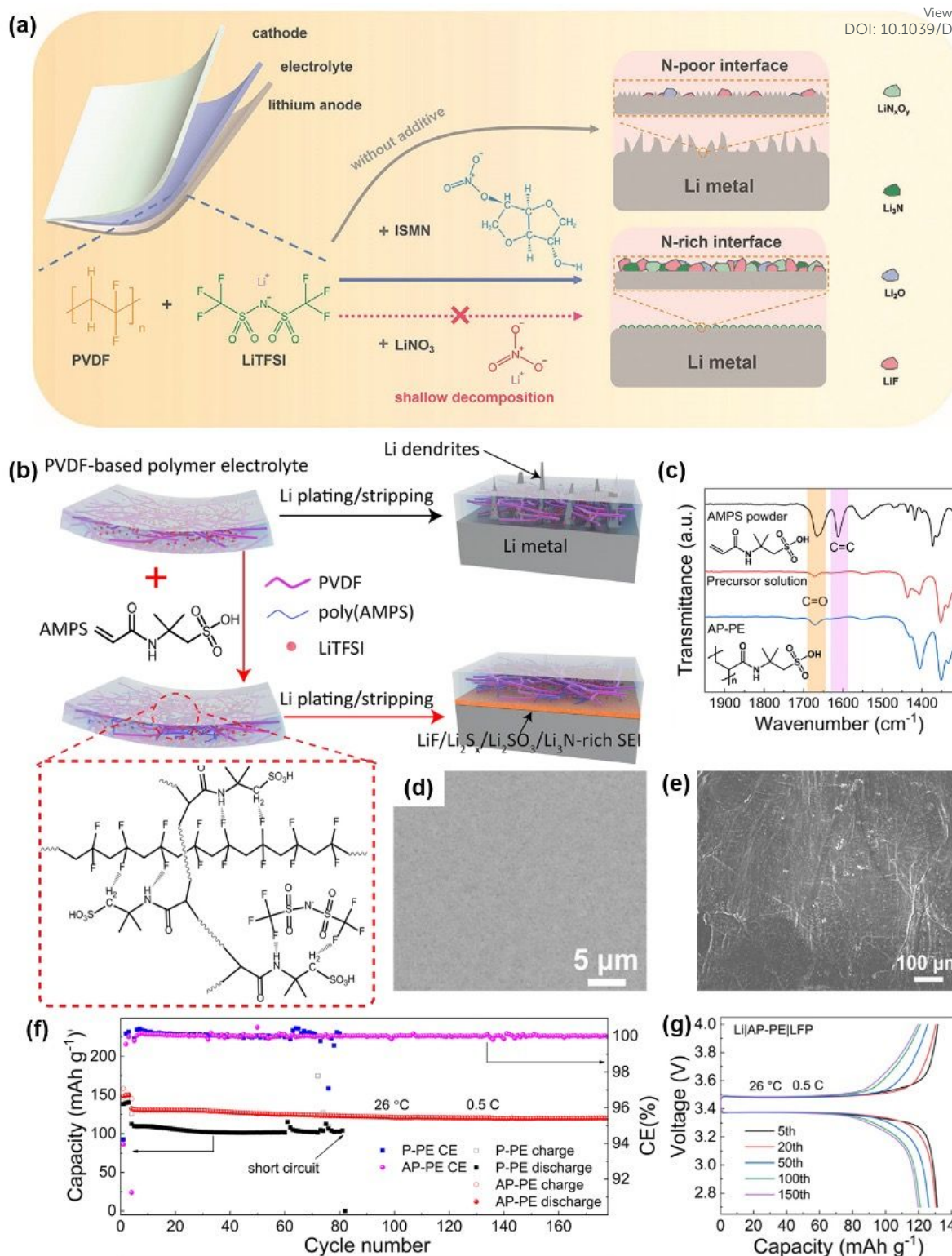
524

525 **Figure 2. Incorporating an interconnected nanowire network to enhance PVDF-based**  
 526 **SSEs.** (a) Illustration of the Li salt dissociation and Li<sup>+</sup> transport facilitated by the coupled  
 527 BTO-LLTO in the PVBL electrolyte. (b) Schematic of Li salt dissociation by a polarized  
 528 dielectric material. (c) The ssNMR spectra of the PVL and (d) PVBL electrolytes before and  
 529 after cycling in a <sup>6</sup>Li symmetric cell, with (e) corresponding peak ratios of <sup>6</sup>Li<sup>+</sup> transport paths.  
 530 (f) Ionic conductivities of the PVDF-based electrolytes at 25°C. (g) Long-term cycling  
 531 performance of PVBL in symmetric cells. Reproduced with permission.<sup>54</sup> Copyright  
 532 2017, Nature Nanotechnology, Nature Publishing Group.

533





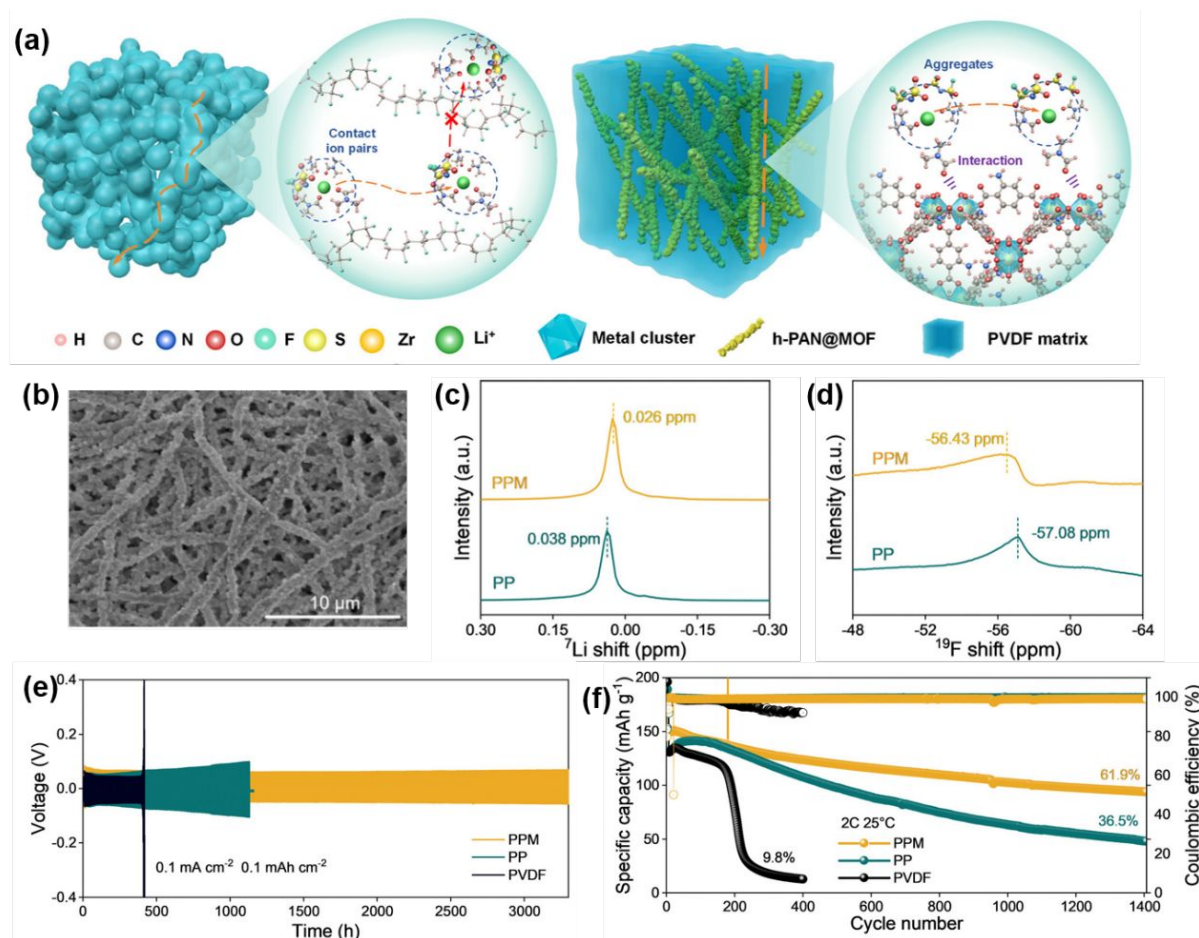


534  
535 **Figure 3. Enhancing PVDF-based SSE through Blending with Organic Fillers.** (a)  
536 Schematic illustration of the modification mechanism using ISMN for PVDF-based SSE.  
537 Reproduced with permission.<sup>49</sup> Copyright 2024, Advanced Functional Materials.  
538 (b) Schematic illustration showing the role of AMPS in promoting Li<sup>+</sup> conduction and  
539 suppressing Li dendrite formation. (c) FTIR spectra of AP-PE. (d) SEM images of the AP-PE  
540 membrane. (e) SEM images of Li electrodes from Li/AP-PE after 500 hours of cycling at 0.1  
541 mA·cm<sup>-2</sup> and 0.1 mAh·cm<sup>-2</sup>. (f) Cycling performance of Li/AP-PE/LFP batteries at 0.5C and



542 (g) The corresponding charge-discharge voltage profiles. Reproduced with permission.<sup>50</sup> Royal Society of Chemistry 2022.

543  
544  
545

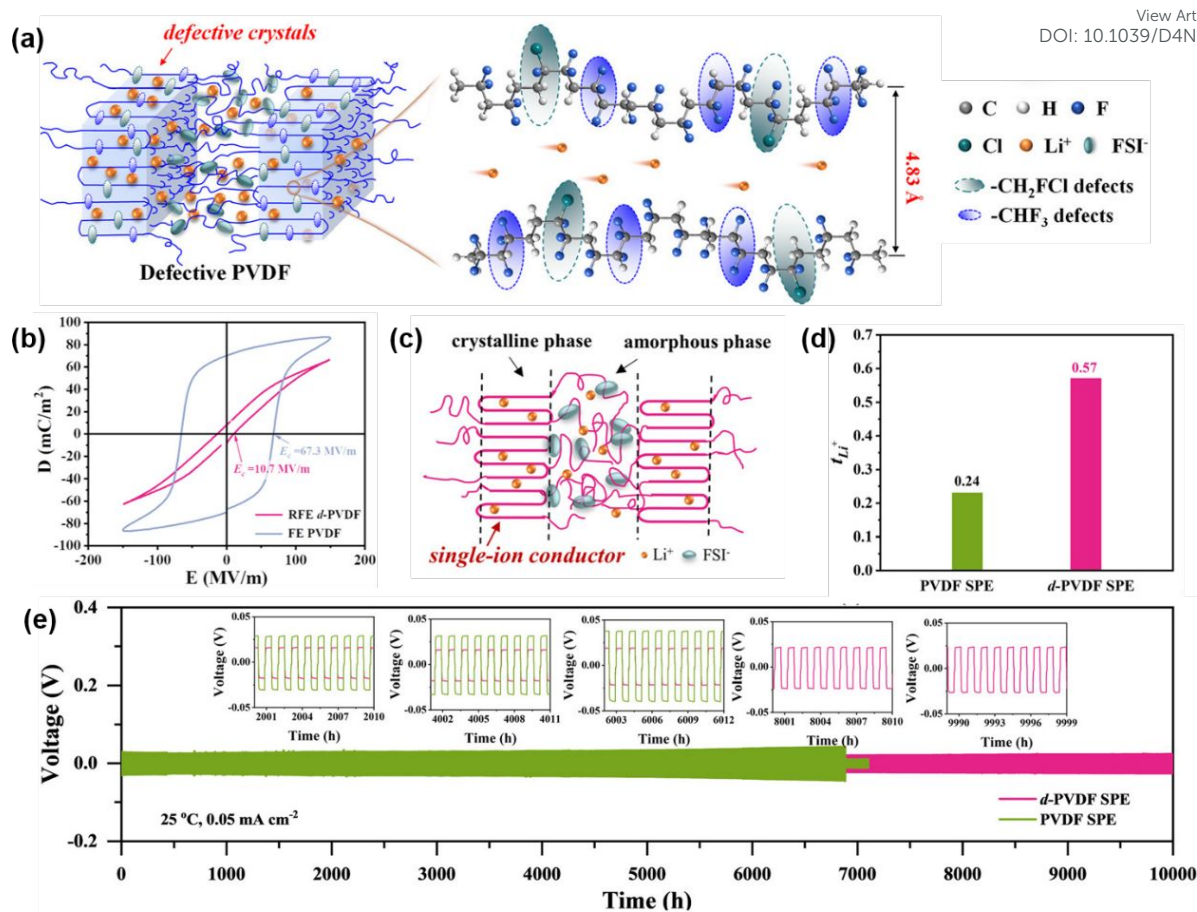


546

547 **Figure 4. Inorganic/Organic Composite Fillers for Enhanced PVDF-based SSE.** (a)  
548 Schematic of ion transport and solvation structures in PVDF and PPM electrolytes. (b)  
549 SEM images of h-PAN@MOF networks. (c) <sup>7</sup>Li ss-NMR spectra. (d) <sup>19</sup>F ss-NMR spectra. (e)  
550 Galvanostatic cycling curves of Li||Li symmetric cells with PVDF, PP, and PPM electrolytes.  
551 (f) Long-term cycling stability of Li||NCM811 cells. Reproduced with permission.<sup>54</sup> Copyright  
552 2023, Nature Nanotechnology, Nature Publishing Group.

553





554

555 **Figure 5. Chemical Modification of PVDF for Enhanced PVDF-based SSE.** (a) Schematic556 illustrating Li<sup>+</sup> transport within d-PVDF crystals. (b) Bipolar D-E loops of PVDF and d-PVDF.557 (c) Schematic representation of Li<sup>+</sup> and FSI<sup>-</sup> location within d-PVDF SPE. (d) Lithium-ion558 transference number ( $t_{Li^+}$ ) comparison between PVDF and d-PVDF SPE. (e) Cycling

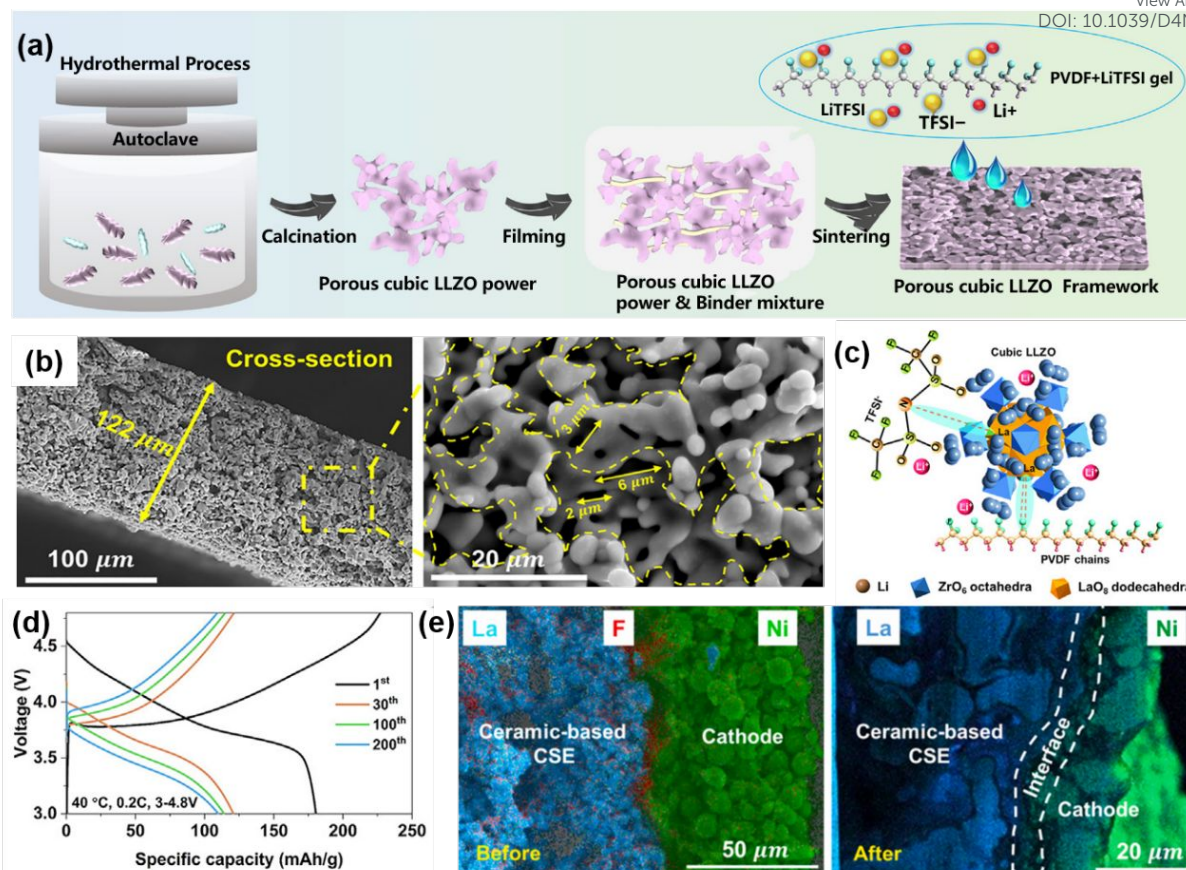
559 performance of Li//Li symmetrical cells with d-PVDF and PVDF SSE. Reproduced with

560 permission.<sup>52</sup> Copyright 2024, Energy & Environmental Science.

561







562

563 **Figure 6. Additional Strategies for Enhancing the Performance of PVDF-based SSE.** (a)  
 564 Schematic illustration of ceramic-based CSE. (b) Cross-sectional SEM image and magnified  
 565 view of the selected region of the CSE. (c) Illustration of the interactions between PVDF-  
 566 LiTFSI CSE and porous LLZO framework. (d) Charge-discharge voltage profiles of a  
 567 Li/ceramic-based CSE/NCM622 solid-state battery. (e) Cross-sectional SEM and  
 568 corresponding EDS mappings of the SSB before and after cycling at 3-4.8V. Reproduced with  
 569 permission.<sup>53</sup> Copyright 2024, Cell Reports Physical Science.

570

571



572 **Table 1:** Summary of Synthesis Methods and Performance of PVDF-based Solid-State  
 573 Lithium Metal Batteries (SSLMBs).

Electrolyte	Synthetic methods	$\sigma^a$ (mS cm <sup>-1</sup> )	$t_{Li^+}^b$	LSV <sup>c</sup> (V)	MS <sup>d</sup> (Mp a)	Lifespan <sup>e</sup> h [F <sub>1</sub> <sup>f</sup> (mA cm <sup>-2</sup> ), F <sub>2</sub> <sup>f</sup> (mAh cm <sup>-2</sup> )]	Battery configuration	performance	Ref
<b>Inorganic filler</b>									
<b>Nanoparticles</b>									
PVDF/LiClO <sub>4</sub> /DMF/ Li <sub>6.75</sub> La <sub>3</sub> Zr <sub>1.75</sub> Ta <sub>0.25</sub> O <sub>12</sub>	Solution-casting method	0.5	/	/	5.92	160(0.05/0.025)	LiCoO <sub>2</sub> /Li	150,98% (120 cycles, 0.4 C)	39
PVDF/LiTFSI/DMF/ Li <sub>1.3</sub> Al <sub>0.3</sub> Ti <sub>1.7</sub> (PO <sub>4</sub> ) <sub>3</sub>	Solution-casting method	0.244	0.52	4.8	/	3000(0.1)	LiNi <sub>0.6</sub> Co <sub>0.2</sub> Mn <sub>0.2</sub> O <sub>2</sub> /Li	125, 80% (400 cycles, 0.5 C)	40
PVDF/LiFSI/DMF/SiO <sub>2</sub>	Solution-casting method	0.481	0.59	/	64	11000(0.1,0.1)	LiNi <sub>0.8</sub> Mn <sub>0.1</sub> C <sub>0.1</sub> O <sub>2</sub> /Li	173, (300 cycles, 0.5C)	41
PVDF/LiFSI/DMF/ NaNbO <sub>3</sub>	Solution-casting method	0.556	0.49	4.7	/	2800(0.1,0.1)	LiNi <sub>0.8</sub> Mn <sub>0.1</sub> C <sub>0.1</sub> O <sub>2</sub> /Li	177, 67.7% (1500 cycles, 1 C)	42
PVDF/LiTFSI/DMF/BiFe	Casting and scraping method	0.139	0.35	4.7	/	2500(0.1,0.1)	LiNi <sub>0.8</sub> Mn <sub>0.1</sub> C <sub>0.1</sub> O <sub>2</sub> /Li	141.7, 89% (400 cycles, 0.3C)	43
PVDF/LiTFSI/NMP/ Li <sub>0.2</sub> Zr(PO <sub>4</sub> ) <sub>3</sub>	Solution-casting method	0.0576	0.73	4.73	/	2000 (0.04)	Li <sub>4</sub> Ti <sub>5</sub> O <sub>15</sub> /Li	133, 88% (20, 0.1C)	55
PVDF/LiTFSI/DMF/ Li <sub>0.2</sub> Zr(PO <sub>4</sub> ) <sub>3</sub>	Solution-casting method	0.228	/	5.2	/	600(0.1)	LiNi <sub>0.5</sub> Co <sub>0.2</sub> Mn <sub>0.3</sub> O <sub>2</sub> /Li	150,88.5% (100 cycles , 0.1C)	56
PVDF/LiFSI/DMF/ Li <sub>6.75</sub> La <sub>3</sub> Zr <sub>1.75</sub> Ta <sub>0.1</sub> Nb <sub>0.4</sub> O <sub>12</sub>	Solution-casting method	0.105	0.66	4.8	/	400(0.1,0.1)	LiNi <sub>0.8</sub> Mn <sub>0.1</sub> C <sub>0.1</sub> O <sub>2</sub> /Li	137, (80cycles,0.3C)	57
PVDF/LiTFSI/DMF/ Li <sub>6.75</sub> La <sub>3</sub> Zr <sub>1.75</sub> Ta <sub>0.1</sub> Nb <sub>0.4</sub> O <sub>12</sub>	Solution-casting method	0.129	0.32	/	/	400(0.2,0.2)	LiNi <sub>0.8</sub> Mn <sub>0.1</sub> C <sub>0.1</sub> O <sub>2</sub> /Li	118.5, 93% (200 cycles , 0.5C)	58
PVDF/LiFSI/DMF/MS	Solution-casting method	0.45	0.47	4.6	/	5100(0.1,0.1)	LiNi <sub>0.8</sub> Mn <sub>0.1</sub> C <sub>0.1</sub> O <sub>2</sub> /Li	178.5, 92.7% (500 cycles , 1C)	59
PVDF/LiClO <sub>4</sub> /DMF/Mg, Ag <sub>2</sub> S <sub>2</sub> O <sub>10</sub> (OH)	Casting and scraping method	0.12	0.54	/	4.7	100(0.05,0.05)	Ni <sub>1/3</sub> Mn <sub>1/3</sub> CO <sub>1/3</sub> O <sub>2</sub> /Li	117.6, 97% (200 cycles , 0.3C)	60
<b>Nanowire</b>									
PVDF/LiTFSI/NMP/ Li <sub>0.33</sub> La <sub>0.55</sub> TiO <sub>3</sub>	Solution-casting method	0.53	/	5.1	9.5	300(0.2,0.2)	LiFePO <sub>4</sub> /Li	121, 99% (100 cycles,1C)	45
PVDF/LiFSI/DMF- Li <sub>0.33</sub> La <sub>0.55</sub> TiO <sub>3-x</sub>	Solution-casting method	0.82	0.57	/	2.11	1900(0.1,0.1)	LiNi <sub>0.8</sub> Mn <sub>0.1</sub> C <sub>0.1</sub> O <sub>2</sub> /Li	180, 70% (1000 cycles,1C)	54
PVDF/LiClO <sub>4</sub> /DMF/V <sub>2</sub> O <sub>5</sub>	Solution-casting method	2.2	0.58	5.2	/	2500(0.5,0.5)	LiFePO <sub>4</sub> /Li	150, 95.3% (300 cycles , 0.1C)	61
PVDF/LiTFSI/DMF/ Li <sub>0.33</sub> La <sub>0.55</sub> TiO <sub>3-x</sub>	Casting and scraping method	0.29	0.75	/	49	400(0.5,0.5)	LiFePO <sub>4</sub> /Li LiNi <sub>0.8</sub> Mn <sub>0.1</sub> C <sub>0.1</sub> O <sub>2</sub> /Li	148, 80% (300 cycles,1C) 149, 70% (200 cycles,1C)	62
PVDF/LiTFSI/DMF/Li/ Li <sub>0.33</sub> La <sub>0.55</sub> TiO <sub>3-x</sub>	Casting and scraping method	0.44	0.33	4.9	/	300(0.1,0.1)	LiFePO <sub>4</sub> /Li	167, 96% (250 cycles,0.5C)	63
<b>Nanosheet</b>									
PVDF/LiFSI/DMF/g- C <sub>3</sub> N <sub>4</sub>	Solution-casting method	0.69	0.49	4.7	11.2	2200(0.1,0.1)	LiNi <sub>0.8</sub> Mn <sub>0.1</sub> C <sub>0.1</sub> O <sub>2</sub> /Li	146.5, 76.6% (1700 cycles,1C)	64
PVDF/LiODFB/DMF/PC	Casting and scraping method	0.118	/	4.75	4.3	160(0.1,0.1)	LiCoO <sub>2</sub> /Li	125, 84% (300cycles,0.1C)	48
PVDF/LiTFSI/NMP/ISM	Solution-casting method	0.44	0.5	4.92	/	5000(0.2,0.1)	LiFePO <sub>4</sub> /Li	154, 88.9% (500cycles,0.5C)	49
PVDF/LiTFSI/NMP/h- BN	Solution-casting method	0.29	0.62	5.24	3.45	1200(0.1,0.1)	LiFePO <sub>4</sub> /Li	121.4, 96% (160 cycles,0.2C)	65
<b>Organic filler</b>									
PVDF/LiFSI/DMF/PAA	Solution-casting method	0.09	/	4.64	/	900(0.44,0.22)	LiCoO <sub>2</sub> /Li	125, 97% (1000cycles,0.1C)	66
PVDF/LiTFSI/DMSO /AMPS	Solution-casting method	0.22	0.49	4.7	/	2100(0.1,0.1)	LiFePO <sub>4</sub> /Li	127.6, 90.8% (220cycles,1C)	50
PVDF/LiTFSI/DMF/TFB Q	Solution-casting method	0.239	0.42	5.0	/	2000(0.1,0.1)	LiNi <sub>0.6</sub> Co <sub>0.2</sub> Mn <sub>0.2</sub> O <sub>2</sub> /Li	150, 80% (180cycles,0.2C)	67
PVDF/LiTFSI/DMF/MgP FPAA	Casting and scraping method	0.14	0.34	4.8	/	2400(0.2,0.2)	LiFePO <sub>4</sub> /Li	120, 74.9% (1500cycles,5C)	68
PVDF/LiTFSI/DMF/HFA	Casting and scraping method	0.241	/	4.9	/	1700(0.1,0.1)	LiNi <sub>0.6</sub> Co <sub>0.2</sub> Mn <sub>0.2</sub> O <sub>2</sub> /Li	176.8, 80% (600cycles,0.2C)	69
PVDF/LiFSI/DMF/FEC/	Solution-casting	0.479	0.43	4.6	6.5	3000(0.1,0.1)	LiFePO <sub>4</sub> /Li	148, 84%	70

LIDFP	method									
									(400cycles, 1C)	New Article Online DOI: 10.1039/D4NR04583A
<b>Organic/Inorganic filler</b>										
PVDF/LiFSI/DMF-h-PAN@MOF	Solution-casting method	1.03	/	4.45	20.8	3200(0.1,0.1)	LiNi <sub>0.8</sub> Mn <sub>0.1</sub> Co <sub>0.1</sub> O <sub>2</sub> /Li	150, 61.9% (1400 cycles, 2 C)		71
PVDF/PVAC/LiTFSI/LiBOB/DMF/Li <sub>6.4</sub> La <sub>3</sub> Zr <sub>1.4</sub> Ta <sub>0.6</sub> O <sub>12</sub>	Casting and scraping method	0.496	0.57	5.4	6	1300(0.1,0.1)	LiFePO <sub>4</sub> /Li	145, 92.3% (220cycles,0.5C)		72
PVDF/LiTFSI/NMP/ZIF-90	Casting and scraping method	0.62	0.48	/	2.1	1000(0.05,0.05)	LiFePO <sub>4</sub> /Li	120, 95% (300cycles,1C)		73
<b>Other strategy</b>										
PVDF-OH/LiTFSI/DMSO	Solution-casting method	0.71	/	/	16.1	1000(0.1,0.1)	LiFePO <sub>4</sub> /Li	145.9, 85.4% (1000cycles,0.5C)		51
P(VDF-CHF <sub>3</sub> -CH <sub>2</sub> FCI)/LiFSI/DMF	Solution-casting method	0.78	0.57	4.4	/	11000(0.05,0.05)	LiNi <sub>0.8</sub> Mn <sub>0.1</sub> Co <sub>0.1</sub> O <sub>2</sub> /Li	154, 94.9% (300 cycles, 1C)		52
PVDF/LiTFSI/NMP/Li <sub>6.1</sub> A <sub>0.3</sub> E <sub>0.3</sub> Zr <sub>2</sub> O <sub>12</sub> framework	Immersing method	0.437	0.72	5.08	/	1000(0.1,0.1)	LiNi <sub>0.6</sub> Co <sub>0.2</sub> Mn <sub>0.2</sub> O <sub>2</sub> /Li	160, 90% (200 cycles, 0.2C)		53
PS-D741/LiClO <sub>4</sub> /DMF	Casting and scraping method	0.12	/	4.9	/	1000(0.1,0.1)	LiFePO <sub>4</sub> /Li	100, 80% (500cycles,0.5C)		74
P(VDF-TrFE-CTFE)/LiFSI/DMF	Solution-casting method	0.31	0.33	4.6	/	1200(0.05,0.05)	LiFePO <sub>4</sub> /Li	146, 98.5% (150cycles,0.5C)		75

574 <sup>(a)</sup>Conductivity (room temperature).

575 <sup>(b)</sup>Ion transference number.

576 <sup>(c)</sup>Linear sweep voltammetry testing electrochemical stability.

577 <sup>(d)</sup>Mechanical strength.

578 <sup>(e)</sup>time (h); <sup>(f)</sup>F<sub>1</sub>: current density (mA cm<sup>-2</sup>); F<sub>2</sub>: specific area capacity (mAh cm<sup>-2</sup>).

579





### Data availability statements

No primary research results, software or code have been included and no new data were generated or analyzed as part of this review.

